Angle-domain sensitivity kernels for migration velocity analysis: comparison between theoretically derived and directly measured

Yaofeng He and Xiao-Bi Xie, IGPP, University of California at Santa Cruz, Santa Cruz, CA 95064, USA.*
Hui Yang, Formerly University of California at Santa Cruz; presently LandOcean Energy Service Inc., Beijing, 100084, China.

Summary

Sensitivity kernels for wave equation based migration velocity analysis in local angle-domain are formulated. These sensitivity kernels serve as operators to backproject the residual moveout in local angle-domain common image gathers to migration models for velocity updating. To validate the theoretical formulation, we directly measure sensitivity kernels using a perturb-measuring approach. For single-shot data, the theoretical sensitivity kernels are consistent with those directly measured. For multi-shot data, the local angle domain sensitivity kernels are approximated by stacking the corresponding single-shot sensitivity kernels.

Introduction

Velocity model building is crucial for prestack depth migration. There are two types of velocity model building approaches: those working in the data space, i.e., by minimizing the differences between the synthetic data and real observations; and those working in the image space, i.e., minimizing the incoherence in migrated images.

Among all the data-space methods, ray tomography has been widely used and efforts have been put to improve the resolution for the past decades both in global and exploration seismology (Woodward et al., 2008). Full waveform inversion is currently a hot issue though limited to low frequency data and requires formidable computation (Tarantola, 1984; Pratt et al., 1998; Pratt, 1999). An alternative approach in between the ray tomography and full waveform inversion is the sensitivity kernel based tomography, where the kernels are used to backproject the phase and amplitude differences, usually for specific phases, to velocity anomalies. This method naturally embraces the characteristics of wave phenomena and can achieve high-resolution results (Dahlen et al., 2000; Tromp et al., 2005; Zhao et al., 2005).

Alternatively, the image-space method, i.e., the migration velocity analysis (MVA), concerns the flatness of local coherent events in common image gathers (CIGs). The CIG is an assembly of partial images indexed by different parameters relating to the data type, the migration method or the image condition. For example, based on type of sources used, the CIG can be indexed by shot, surface offset or plane-wave source parameters. Based on the migration method and image condition, the CIG can be indexed by local offset or local angles. It is possible for CIG to have double indexes, for example, calculating angle-domain partial image from shot records makes the CIG having both shot and angle indexes. It is not trivial to calculate local angle-domain partial images from wave-equation based migration. Several approaches have been proposed for this purpose, e.g., extracting the angle-domain image from common offset migration (de Bruin et al., 1990; Wang et al., 1995; Reshef, 2001; Chauris et al., 2002), local image matrix (Xie and Wu, 2002; Wu and Chen, 2003), or space-time shifted partial images (Rickett and Sava, 2002; Sava and Fomel, 2003; Sava and Biondi, 2004; Singh et al., 2008). The relationships between these local angle-domain CIGs are yet to be investigated. Nevertheless, the common basic principle to conduct the MVA is that local coherent events in CIGs should be flat if a right migration velocity is used. The measurement of incoherencies in CIGs is residual moveout (RMO) which reflects the errors in velocity model. Correctly converting RMOs to model space for velocity updating remains a challenge for MVA. Ray-based backprojection evenly distributes the velocity error along narrow rays. Instead, wavepath tomography (Fliedner and Bevc, 2008) backprojects RMOs along the wavepaths. de Hoop et al. (2006) discussed the sensitivity kernel for reflection waves based on the double square root equation. Sava and Vlad (Sava and Vlad, 2008) studied the relation between image perturbation and anomaly in velocity model through numerical implementation of migration operator.

Recently, a wave equation based sensitivity kernel is derived for the RMOs in shot-indexed CIGs (Xie and Yang, 2007, 2008a). This sensitivity kernel is consistent with the wave-equation-based shot-profile PSDM. Velocity perturbation can be obtained by inversion based on this sensitivity kernel. In this paper, following Xie and Yang (2008a), we study the sensitivity of the local angle-domain CIG to errors in migration velocity models. Based on scattering theory, the sensitivity kernel for angle-domain CIG is derived and compared with the directly measured sensitivity map.

Sensitivity kernels for single-shot local-angle CIG

We formulate the sensitivity kernel which links the local angle-domain common image gather (LADCIG) to errors in migration velocity model. Following Xie and Yang (Xie and Yang, 2007, 2008a, b), we start from the angle-domain partial imaging condition for a single-shot record (Xie and Wu, 2002; Wu and Chen 2003)

Angle domain sensitivity kernels for MVA

$$I_0(\theta_g,\theta_s;r_I\,|\,r_s,\omega)=u_D^0(\theta_s;r_I\,|\,r_s,\omega)\overline{u_U^0}(\theta_g;r_I\,|\oint r_g,\omega) \quad (1)$$

where $I_0(\theta_g,\theta_s;r_I\,|\,r_s,\omega)$ is the partial image, θ_s and θ_g are incident and scattering angles, r_s and r_I are locations of the source and image point, and u_D^0 and u_U^0 are up- and down-going waves from source and receivers, the superscript zero denotes these waves are calculated in the initial model and the bar means complex-conjugate. The up-going wave is the back-propagated surface data. The integral indicate all the data within the acquisition aperture are used for down-ward extrapolation.

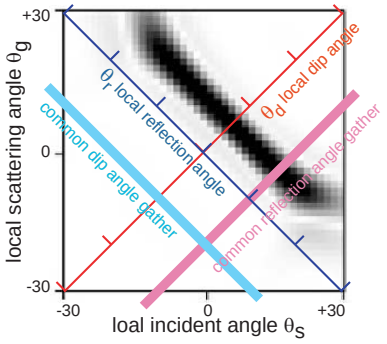

Figure 1: The structure of a local image matrix and relations between different local angles.

To obtain the angle-domain partial images, both the down- and up-going waves are decomposed into local plane waves (local beams) before applying the traditional cross-correlation imaging condition. In this way the partial images form a local image matrix (Wu and Chen, 2003) (Figure 1), within which, each element is composed of a pair of local beams, one from the source side with incident angle θ_s and another from the receiver side with scattering angle θ_g. The local incident/scattering angle system can be transformed into local reflection/dipping angle system through (Xie and Wu, 2002)

$$\theta_d=\left(\theta_s+\theta_g\right)/2;\ \theta_r=\left(\theta_g-\theta_s\right)/2, \quad (2)$$

where θ_r and θ_d are local reflection angle and local dip angle, respectively. The dip angle θ_d can be estimated from the stacked image or from the energy distribution in local image matrix (Wu and Chen, 2003). Given the image point r_I and dip angle θ_d, the transform (2) converts the local image matrix into a single-shot LADCIG

$$I_0(\theta_r;r_I\,|\,r_s,\omega)=u_D^0(\theta_s;r_I\,|\,r_s,\omega)\overline{u_U^0}(\theta_g;r_I\,|\oint r_g,\omega)\,. \quad (3)$$

If the receiver array forms a full aperture acquisition system, the back-propagation of recorded data should reproduce the backscattered wave from the target (time reversal). The backscattered wave can be solely determined by the source and subsurface structures. The integral over receivers in equations (1) and (3) can be replaced by the source index.

$$I_0(\theta_r;r_I\,|\,r_s,\omega)=u_D^0(\theta_s;r_I\,|\,r_s,\omega)\overline{u_U^0}(\theta_g;r_I\,|\,r_s,\omega)\,. \quad (4)$$

To pick the RMO from common reflection angle CIG, we compare the image in the initial model (equation 4) with the image in the accurate velocity model, i.e.,

$$I(\theta_r;r_I\,|\,r_s,\omega)=u_D(\theta_s;r_I\,|\,r_s,\omega)\overline{u_U}(\theta_g;r_I\,|\,r_s,\omega)\,. \quad (5)$$

Based on Rytov approximation for scattering waves (Jocker et al., 2006; Wu et al., 2007), the phase difference between the two images can be obtained as

$$\begin{aligned}\delta\varphi(\theta_r;r_I\,|\,r_s,\omega)&=\delta\varphi_D(\theta_s;r_I\,|\,r_s,\omega)+\delta\varphi_U(\theta_g;r_I\,|\,r_s,\omega)\\&\simeq\mathrm{Im}\left\{\frac{\delta u_D(\theta_s;r_I\,|\,r_s,\omega)}{u_D^0(\theta_s;r_I\,|\,r_s,\omega)}\right\}+\mathrm{Im}\left\{\frac{\delta\overline{u_U}(\theta_g;r_I\,|\,r_s,\omega)}{\overline{u_U^0}(\theta_g;r_I\,|\,r_s,\omega)}\right\},\end{aligned} \quad (6)$$

where $\delta u=u-u^0$ is the scattered wave due to the velocity difference between the initial and accurate models. Using the scattering theory, we approximate δu by (Woodward, 1992; Jocker et al., 2006)

$$\delta u_{D,U}(\theta;r_I\,|\,r_s,\omega)=2\int k_0^2G_{D,U}^0(r\,|\,r_s,\omega)\delta v(r)G^0(\theta;r_I\,|\,r,\omega)dr\,, \quad (7)$$

where $G_{D,U}^0(r_2\,|\,r_1,\omega)$ represents the Green's function for down- and up-going waves with a source located at r_1 and a receiver at r_2, δv is the relative velocity perturbation. $G^0(\theta;r_2\,|\,r_1,\omega)$ is the local plane wave Green's function which calculates a local plane wave along direction θ at receiver point r_2 generated by a source located at r_1. Both these Green's functions are calculated in the background model. Substituting (7) in (6), we obtain the equation relating the phase delay in the image to the velocity error

$$\begin{aligned}\delta\varphi(\theta_r;r_I\,|\,r_s,\omega)&=\int K_D(\theta_s,r;r_I\,|\,r_s,\omega)\delta v(r)dr\\&\quad+\int K_U(\theta_g,r;r_I\,|\,r_s,\omega)\delta v(r)dr,\end{aligned} \quad (8)$$

where K_D and K_U are sensitivity kernels for down- and up-going waves and can be written as

$$K_D(\theta_r,r;r_I\,|\,r_s,\omega)=\mathrm{Im}\left(2k_0^2\frac{G_D^0(r\,|\,r_s,\omega)G^0(\theta_s;r_I\,|\,r,\omega)}{G_D^0(\theta_s;r_I\,|\,r_s,\omega)}\right), \quad (9)$$

and

$$K_U(\theta_r,r;r_I\,|\,r_s,\omega)=\mathrm{Im}\left(2k_0^2\frac{\overline{G_U^0}(r\,|\,r_s,\omega)G^0(\theta_g;r_I\,|\,r,\omega)}{\overline{G_U^0}(\theta_g;r_I\,|\,r_s,\omega)}\right). \quad (10)$$

The correspondent broadband kernels can be obtained by stacking single-frequency kernels (Xie and Yang, 2008b)

$$K_U^B(\theta_r,r;r_I\,|\,r_s)=\int\frac{W(\omega)}{\omega}K_U(\theta_r,r;r_I\,|\,r_s,\omega)d\omega\,, \quad (11)$$

$$K_D^B(\theta_r,r;r_I\,|\,r_s)=\int\frac{W(\omega)}{\omega}K_D(\theta_r,r;r_I\,|\,r_s,\omega)d\omega\,. \quad (12)$$

$W(\omega)$ is a weighting function depends on the source spectrum. Note that, in equations (9)-(10), the Green's function $G^0(\theta; r_I \mid r, \omega)$ needs to be calculated between every space location r and the image point r_I. In addition, the plane wave decomposition needs be applied at the image point. To replace these time consuming calculations, we apply the reciprocity to the Green's function. Instead of shooting waves from every space location to the image point, we actually shoot one local plane wave along direction θ from the image point to the entire model space.

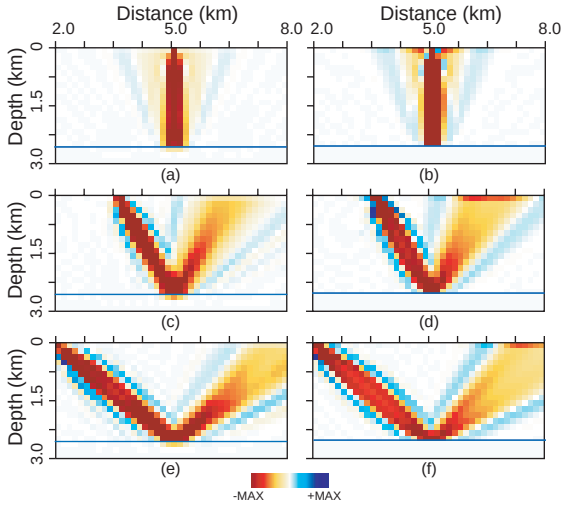

Figure 2: Comparison of direct measured (left column) and theoretically calcualted (right column) sensitivity kernels.

Fidelity of the theoretical sensitivity kernel

To test the fidelity of the sensitivity kernel calculation, we utilize the perturb-measuring procedure similar to Xie and Yang (2008a). First, we use the finite-difference method to generate a reflection data set in an accurate model. Second, we use a local cosine beamlet propagator (Wu et al., 2008) to migrate the synthetic data in the accurate velocity model and assemble the common image gathers, called true CIGs, at selected image points. In the third step, we perturb the velocity model by adding a known positive anomaly to the accurate model. The anomaly is a small circular patch with a radius that is one tenth of the dominant wavelength and the velocity perturbation is 5%. To directly measure how the velocity error can affect the image, we use this perturbed model to migrate the synthetic data and assemble the CIGs at the same image points. Then we move the patch through the entire model space and repeat the migration for each location. We measure the RMOs by calculating the depth difference between the perturbed CIGs and true CIGs. The last step, we put the RMO values at the locations of the corresponding perturbations to generate a sensitivity map. In this way, we achieve a directly measured "sensitivity kernel" which is completely independent of any theoretical derivations. As long as the size of the patch and the velocity perturbation are small, this kernel is accurate and can be used to check the theoretically derived kernel.

For a single-shot data set, the CIGs are indexed with shot, image point, and reflection angle, so are the corresponding sensitivity kernels. We compare the directly measured kernels with the kernels calculated from equations (11) and (12). A generalized screen propagator (Xie and Wu, 1998) is adopted for calculating the kernels.

As a simple example, we use a constant velocity model to investigate the fidelity of the single-shot theoretical sensitivity kernel. The background velocity is 3.5 km/s. A flat reflector is located at depth 2.5 km. Figure 2 compares the theoretically calculated (left column) and directly measured (right column) sensitivity kernels for an image point located at (5.0, 2.5) km, where different rows are for different source locations and angles. Shown in Figure 2a is the directly measured sensitivity kernel for a shot located at (5.0, 0.0) km and a reflection angle $\theta_r = 0^\circ$. The theoretical sensitivity kernel is shown in Figure 2b. Figures 2c and 2d compare the sensitivity kernels for $\theta_r = 30^\circ$ and $r_s = (3.57, 0.0)\,\text{km}$. Figures 2e and 2f are for $\theta_r = 50^\circ$, $r_s = (2.0, 0.0)\,\text{km}$. We see that from each pair of kernels the theoretical kernel matches the measured one very well. Considering the fact that the local dip angle is zero, the reflection angle mirrors the incident angle. The source locations have been chosen to maximize the down-going wave energy along the corresponding incident directions.

Sensitivity kernel for multi-shot LADCIGs

In practice, the LADCIGs are calculated from multi-shot data by stacking angle domain partial images from individual shots (Xie and Wu, 2002; Wu and Chen, 2003). This process eliminates the shot index and leaves the stacked LADCIGs have two indices — reflection angle and common depth point. We perform direct measurement of multi-shot sensitivity kernels in a way similar to that used for single-shot kernels in the previous section. We use the same constant velocity model and arrange 51 sources from 2.0 to 8.0 km along the surface with a space of 0.12 km. The receiver array covers the entire surface with a spatial interval 0.01 km. A 17.5 Hz Ricker wavelet is used in the calculation. The radius of the circular velocity perturbation is 0.015 km and the perturbation is 5% of the background velocity. Shown in Figure 3a is a sensitivity kernel for an image point located at (5.0, 2.5) km and a reflection angle

Angle domain sensitivity kernels for MVA

$\theta_r = 30^\circ$. The main lobes of the kernel are negative (red) and fall along the ray trajectories associated with the local reflection angle. The most sensitive region becomes wider when away from the image point. On both sides of the main lobe there are positive regions (blue) which are not predicted by the ray theory. Although the shots are distributed along the entire surface, only those with favorite directions actually contribute to this kernel, indicating the local plane wave analysis has strong angle selection power.

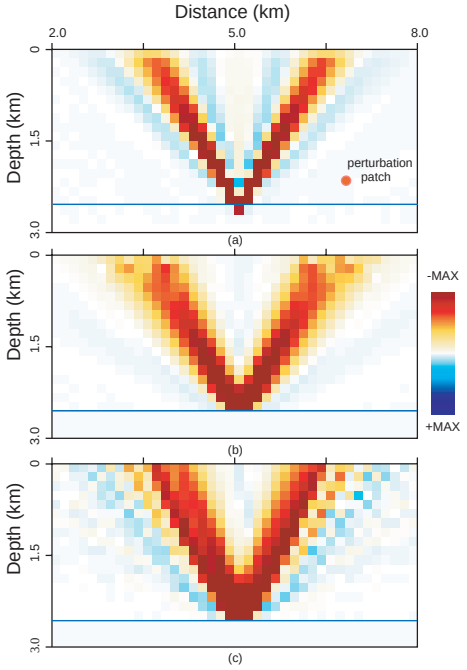

Figure 3: Comparison among directly measured and theoretical sensitivity kernels for common reflection angle CIGs, with (a) direct mesurement, (b) theoretical kernel by stacking single-shot kernels and (c) theoretical kernel by stacking plane-wave source kernels.

If we follow the method that actually used for calculating the LADCIG, the multi-shot sensitivity kernel for LADCIG should be calculated by first stacking the angle-domain partial images, i.e.,

$$\delta\varphi(\theta_r; r_I \mid r_s, \omega) = \arg\left\{\frac{I(\theta_s, \theta_g; r_I, \omega)}{I_0(\theta_s, \theta_g; r_I, \omega)}\right\} = \arg\left\{\frac{\sum_{r_s}\left(u_D(\theta_s; r_I \mid r_s, \omega)\overline{u_U}(\theta_g; r_I \mid r_s, \omega)\right)}{\sum_{r_s}\left(u_D^0(\theta_s; r_I \mid r_s, \omega)\overline{u_U^0}(\theta_g; r_I \mid r_s, \omega)\right)}\right\} \quad (13)$$

where the summations are applied to angle domain partial images from different sources. However, these summations cannot be performed in calculating the theoretical sensitivity kernels because the images are not actually generated in kernel calculation. Instead, we calculate the multi-shot kernel by stacking the single shot kernels. By investigating equations (6), (8) and (13), we write the multi-shot sensitivity kernel for LADCIG

$$K^B(\theta_r, r_I) \approx \sum_{r_s} W(r_s, \theta_r)\left[K_D^B(\theta_r, r; r_I \mid r_s) + K_U^B(\theta_r, r; r_I \mid r_s)\right] \quad (14)$$

where $W(r_s, \theta_r)$ is a weighting function adopted for simulating the selection of the angle-domain analysis. It is indexed by the source r_s and reflection angle θ_r and is proportional to the energy flux along the incident direction at the image point. Note that stacking the kernel is not exactly equivalent to stacking the image and this step should be considered an approximation.

The theoretically calculated multi-shot sensitivity kernel based on equation (14) is shown in Figure 3b. Alternatively, the multiple shots can be phase-encoded and superposed into plane-wave sources, from which the multi-shot sensitivity kernels for LADCIG can also be obtained (Figure 3c). Comparing to the directly measured sensitivity kernel, these theoretical kernels have the similar feature but with noticeable differences, indicating that the actual process of stacking image may not be properly reproduced by stacking the kernels.

Conclusion

We study the sensitivity of LADCIG to migration velocity model errors. This sensitivity is crucial for building an inversion system for MVA based on the LADCIG. We derive the theoretical sensitivity kernel for wave equation based migration velocity analysis in local angle domain. Both directly measured and theoretically calculated kernels are investigated. For single-shot data, the theoretical sensitivity kernels are consistent with those from a brutal force numerical perturb-measurement. For multi-shot data, the theoretical sensitivity kernel is obtained by stacking the single-shot kernels. Future works will focus on improving the fidelity of multi-shot sensitivity kernels.

Acknowledgement

This research is supported by the WTOPI Research Consortium at the University of California, Santa Cruz. The facility support from the W.M. Keck Foundation is also acknowledged.

EDITED REFERENCES

Note: This reference list is a copy-edited version of the reference list submitted by the author. Reference lists for the 2009 SEG Technical Program Expanded Abstracts have been copy edited so that references provided with the online metadata for each paper will achieve a high degree of linking to cited sources that appear on the Web.

REFERENCES

Chauris, H., M. S. Noble, G. Lambare, and P. Podvin, 2002, Migration velocity analysis from locally coherent events in 2-D laterally heterogeneous media, Part II: Applications on synthetic and real data: Geophysics, **67**, 1213–1224.

Dahlen, F.A., S. H. Hung, and G. Nolet, 2000, Frechet kernels for finite-frequency traveltimes - I. Theory: Geophysical Journal International, **141**, 157–174.

de Bruin, C. G. M., C. P. A. Wapenaar, and A. J. Berkhout, 1990, Angle-dependent reflectivity by means of prestack migration: Geophysics, **55**, 1223–1234.

de Hoop, M. V., R. D. van der Hilst, and P. Shen, 2006, Wave-equation reflection tomography: annihilators and sensitivity kernels: Geophysical Journal International, **167**, 1332–1352.

Fliedner, M. M., and D. Bevc, 2008, Automated velocity model building with wavepath tomography: Geophysics, **73**, no. 5, VE195–VE204.

Jocker, J., J. Spetzler, D. Smeulders, and J. Trampert, 2006, Validation of first-order diffraction theory for the traveltimes and amplitudes of propagating waves: Geophysics, **71**, T167–T177.

Pratt, R. G., 1999, Seismic waveform inversion in the frequency domain, Part 1: Theory and verification in a physical scale model: Geophysics, **64**, 888–901.

Pratt, R. G., C. Shin, and G. J. Hicks, 1998, Gauss-Newton and full Newton methods in frequency-space seismic waveform inversion: Geophysical Journal International, **133**, 341–362.

Reshef, M., 2001, Some aspects of interval velocity analysis using 3-D depth-migrated gathers: Geophysics, **66**, 261–266.

Rickett, J. E., and P. C. Sava, 2002, Offset and angle-domain common image-point gathers for shot-profile migration: Geophysics, **67**, 883–889.

Sava, P., and B. Biondi, 2004, Wave-equation migration velocity analysis. I. Theory: Geophysical Prospecting, **52**, 593–606.

Sava, P., and I. Vlad, 2008, Numeric implementation of wave-equation migration velocity analysis operators: Geophysics, **73**, no. 5, VE145–VE159.

Sava, P. C., and S. Fomel, 2003, Angle-domain common-image gathers by wavefield continuation methods: Geophysics, **68**, 1065–1074.

Singh, V.P., B. Duquet, M. Leger, and M. Schoenauer, 2008, Automatic wave-equation migration velocity inversion using multiobjective evolutionary algorithms: Geophysics, **73**, no. 5, VE61–VE73.

Tarantola, A., 1984, Inversion of seismic-reflection data in the acoustic approximation: Geophysics, **49**, 1259–1266.

Tromp, J., C. Tape, and Q. Y. Liu, 2005, Seismic tomography, adjoint methods, time reversal and banana-doughnut kernels: Geophysical Journal International, **160**, 195–216.

Wang, B., K. Pann, and R. A. Meek, 1995, Macro velocity model estimation through model-based globally-optimized residual-curvature analysis: 65th Annual International Meeting, SEG, Expanded Abstracts, 1084–1087.

Woodward, M. J., 1992, Wave-equation tomography: Geophysics, **57**, 15–26.

Woodward, M. J., D. Nichols, O. Zdraveva, P. Whitfield, and T. Johns, 2008, A decade of tomography: Geophysics, **73**, 5–11.

Wu, R.-S., and L. Chen, 2003, Prestack depth migration in angle-domain using beamlet decomposition: Local image matrix and local AVA: 73rd Annual International Meeting, SEG, Expanded Abstracts, 973–976.

Wu, R. S., Y. Z. Wang, and M. Q. Luo, 2008, Beamlet migration using local cosine basis: Geophysics, **73**, no. 5, S207–S217.

Wu, R. S., X. B. Xie, and X. Y. Wu, 2007, One-way and one-return approximations (De Wolf approximation) for fast elastic wave modeling in complex media: Advances in Geophysics, **48**, 265–322.

Xie, X. B., and R. S. Wu, 1998, Improve the wide angle accuracy of screen method under large contrast: 68th Annual International Meeting, SEG, Expanded Abstracts, 1811–1814.

———,2002, Extracting angle domain information from migrated wavefield: 72nd Annual International Meeting, SEG, Expanded Abstracts, 1360–1363.

Xie, X. B., and H. Yang, 2007, A migration-velocity updating method based on the shot-index common image gather and finite-frequency sensitivity kernel: 72nd Annual International Meeting, SEG, Expanded Abstracts, 2767–2771.

———, 2008a, The finite-frequency sensitivity kernel for migration residual moveout and its applications in migration velocity analysis: Geophysics, **73**, no. 6, S241–S249.

———, 2008b, A wave-equation migration velocity analysis approach based on the finite-frequency sensitivity kernel: 78th Annual International Meeting, SEG, Expanded Abstracts, 3093–3097.

Zhao, L., T. H. Jordan, K. B. Olsen, and P. Chen, 2005, Frechet kernels for imaging regional earth structure based on three-dimensional reference models: Bulletin of the Seismological Society of America, **95**, 2066–2080.